Photoinduced valley and electron-hole symmetry breaking in α-T_3 lattice: The role of a variable Berry phase

Bashab Dey and Tarun Kanti Ghosh
Department of Physics, Indian Institute of Technology-Kanpur, Kanpur 208 016, India

(Received 21 June 2018; revised manuscript received 9 August 2018; published 22 August 2018)

We consider an α-T_3 lattice illuminated by intense circularly polarized radiation in the terahertz regime. We present the quasienergy band structure, time-averaged energy spectrum, and time-averaged density of states of an α-T_3 lattice by solving the Floquet Hamiltonian numerically. We obtain exact analytical expressions of the quasienergies at the Dirac points for all values of α and field strength. We find that the quasienergy band gaps at the Dirac point decrease with increase of α. Approximate forms of quasienergy and band gaps at single- and multiphoton resonant points are derived using the rotating wave approximation. The expressions reveal a stark dependence of quasienergy on the Berry phase of the charge carrier. The quasienergy flat band remains unaltered in the presence of radiation for a dice lattice ($\alpha = 1$). However, it acquires a dispersion in and around the Dirac and even-photon resonant points when $0 < \alpha < 1$. The valley degeneracy and electron-hole symmetry in the quasienergy spectrum are broken for $0 < \alpha < 1$. Unlike graphene, the mean energy closely follows the linear dispersion of the Dirac cones until near the single-photon resonant point in the dice lattice. There are additional peaks in the time-averaged density of states at the Dirac point for $0 < \alpha \leqslant 1$.

DOI: 10.1103/PhysRevB.98.075422

I. INTRODUCTION

In recent years, the dynamical effect of an intense ac field on electronic, transport, and optical properties in quantum two-dimensional materials having a Dirac-like spectrum has drawn much interest [1–12]. It is seen that an intense time-periodic field substantially changes the energy-band structure by photon dressing and, consequently, the topological properties of materials. Inducing a gap in Dirac materials is an important issue for electronic devices. A stationary energy gap appears at the Dirac points under a circularly polarized radiation [6,8,9]. Also, the gaps appear in the quasienergy spectrum [10] due to single-photon and multiphoton resonances, which decreases with increase in momentum. Oka and Aoki showed that the photovoltaic Hall effect can be induced in graphene under intense ac field [6], even in the absence of uniform magnetic field. The energy gap at the Dirac point closes as soon as the spin-orbit interaction in the graphene monolayer is taken into account [11]. The optical conductivity of the graphene monolayer under intense field has been reported to show multi-step-like behavior due to sideband-modulated optical transitions [10]. A photo-induced topological phase transition in silicene has been proposed by Ezawa [13]. The photoinduced zero-momentum pseudospin polarization, quasienergy band structure, and time-averaged density of states (DOS) of the charge carriers in monolayer silicene have also been studied [14].

There exists an analogous lattice of graphene [15], known as the α-T_3 lattice, in which quasiparticles are described by the Dirac-Weyl equation. The α-T_3 lattice, as shown in Fig. 1(a), is a honeycomb lattice with two sites (A,B) and an additional site (C) at the center of each hexagon. The C sites are bonded to the alternate corners of the hexagon, say B sites. The hopping parameter between the A and B sites is t and that between the C and B sites is αt. The sites in such a lattice can be subdivided into two categories on the basis of the number of nearest neighbors—*hub* (B) sites with coordination number 6 and *rim* (A,C) sites with coordination number 3. The rim sites form a hexagonal lattice with no bonds among them. The hub sites form a triangular lattice. Each hub site is connected to six rim sites out of which three are equivalent. The hopping parameter alternates between t and αt among the six hub-rim bonds from a single hub site. The $\alpha = 0$ results in the honeycomb lattice resembling monolayer graphene, which corresponds to a Dirac-Weyl system with pseudospin 1/2. On the other hand, $\alpha = 1$ leads to the well-studied T_3 or dice lattice with pseudospin 1 [16–23]. Tuning of α from 0 to 1 gradually allows us to study the continuous changes in the electronic properties of massless fermions.

The dice lattice can naturally be built by growing trilayers of cubic lattices (e.g., $SrTiO_3/SrIrO_3/SrTiO_3$) in the (111) direction [24]. An optical dice lattice can be produced by a suitable arrangement of three counterpropagating pairs of laser beams [19]. The α-T_3 optical lattice can be realized by dephasing one of the pairs of laser beams with respect to the other two [19,25]. The Hamiltonian of the $Hg_{1-x}Cd_xTe$ quantum well can also be mapped to that of the low-energy α-T_3 model with effective $\alpha = 1/\sqrt{3}$ on appropriate doping [26].

Recently, a list of physical quantities such as orbital susceptibility [25], optical conductivity [27–29], magnetotransport properties [26,30–32], Klein tunneling [20,33], and wave-packet dynamics [34] in the α-T_3 lattice has been studied extensively. The Berry phase has become an indispensable ingredient in modern condensed-matter physics due to its strong influence on magnetic, transport, and optical properties [35]. For example, the variation of the orbital susceptibility with α is a direct consequence of the variable Berry phase of the

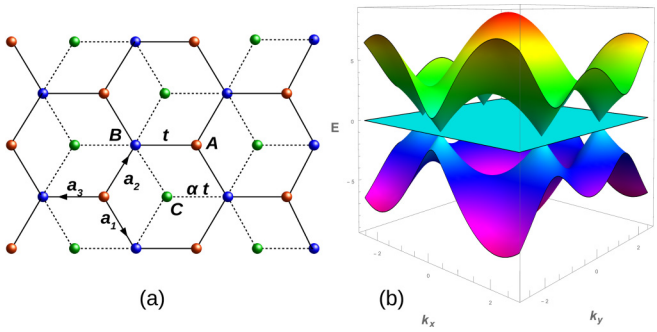

FIG. 1. (a) Sketch of the α-T_3 lattice. (b) Band structure of the α-T_3 lattice using a tight-binding lattice.

α-T_3 lattice [25]. It has been pointed out that the quantization of the Hall plateaus [26,30,31] and behavior of the SdH oscillation [30] change with the Berry phase of the α-T_3 lattice. The Berry phase dependence of the longitudinal optical conductivity of the α-T_3 lattice has also been reported [27].

In this work, we study quasienergy band structure, time-averaged energy spectrum, and time-averaged density of states of the α-T_3 lattice irradiated by circularly polarized light. We provide exact and approximate analytical expressions of the quasienergies at the Dirac points as well as at resonant k points for all values of α, respectively. The valley degeneracy and the electron-hole symmetry are destroyed by the circularly polarized radiation for $0 < \alpha < 1$. We establish a direct connection between the quasienergy spectrum and the variable Berry phase, which is responsible for the broken valley degeneracy. The quasienergy gap at the Dirac point decreases with α. The behaviors of the time-averaged energy and time-averaged density states for $0 < \alpha \leqslant 1$ are appreciably different from that of monolayer graphene.

This paper is organized as follows. In Sec. II, we present preliminary information of the α-T_3 lattice. In Sec. III, we solve the Floquet eigensystem for the α-T_3 lattice driven by circularly polarized light. In particular, we present numerical and analytical results of quasienergy bands and the corresponding band gaps. In Sec. IV, the results of the time-averaged energy spectrum and time-averaged density of states are presented. In Sec. V, we discuss the main results of our study.

II. BASIC INFORMATION OF $\alpha - T_3$ LATTICE

The rescaled tight-binding Hamiltonian of the system considering only nearest-neighbor (NN) hopping is given by

$$H_0(\mathbf{k}) = \begin{pmatrix} 0 & tf^*(\mathbf{k})\cos\phi & 0 \\ tf(\mathbf{k})\cos\phi & 0 & tf^*(\mathbf{k})\sin\phi \\ 0 & tf(\mathbf{k})\sin\phi & 0 \end{pmatrix}, \tag{1}$$

where t is the NN hopping amplitude, α is parameterized by the angle ϕ as $\alpha = \tan\phi$, and $f(\mathbf{k}) = \sum_{j=1}^{3} e^{i\mathbf{k}\cdot\mathbf{a}_j}$. Here, $\mathbf{a}_j$'s are the position vectors of the three nearest neighbors with respect to the rim site. Diagonalizing the Hamiltonian gives three energy bands (E_λ) independent of α [36]: $E_\pm(\mathbf{k}) = \pm t|f(\mathbf{k})|$ and $E_0(\mathbf{k}) = 0$. Here, $\lambda = +1, 0, -1$ correspond to the conduction, flat, and valence bands, respectively. A unique feature of its band structure is that a flat band $E_0(\mathbf{k})$ is sandwiched between two dispersive bands $E_\pm(\mathbf{k})$ which have electron-hole symmetry. The nondispersive band also appears in the Lieb [37–40] as well as kagome [41] models. Recently, the dispersionless flat band has been engineered in a photonic Lieb lattice formed by a two-dimensional array of optical waveguides [42,43]. The flat band remains dispersionless for all values of α and $\mathbf{k}$. On the other hand, the dispersion of the conduction and valence bands is identical to that of graphene. The full band structure is shown in Fig. 1(b).

The low-energy Hamiltonian around the two inequivalent Dirac points $\mathbf{K}$ and $\mathbf{K}'$ can be written as

$$H_0^\mu(\mathbf{k}) = \hbar v_f \mathbf{S}(\alpha)\cdot\mathbf{k}, \tag{2}$$

where $v_f = 3at/(2\hbar)$, $\mathbf{k} = \mu k_x\hat{\mathbf{x}} + k_y\hat{\mathbf{y}}$ with $\mu = \pm 1$ referring to the $\mathbf{K}$ and $\mathbf{K}'$ valleys, respectively, and the components of the spin matrix $\mathbf{S}(\alpha)$ are defined as

$$S_x(\alpha) = \begin{pmatrix} 0 & \cos\phi & 0 \\ \cos\phi & 0 & \sin\phi \\ 0 & \sin\phi & 0 \end{pmatrix}, \tag{3}$$

$$S_y(\alpha) = \begin{pmatrix} 0 & -i\cos\phi & 0 \\ i\cos\phi & 0 & -i\sin\phi \\ 0 & i\sin\phi & 0 \end{pmatrix}. \tag{4}$$

In the vicinity of the two Dirac points, $E_\pm(\mathbf{k})$ are linear in $\mathbf{k}$, i.e., $E_\pm(\mathbf{k}) = \pm\hbar v_f|\mathbf{k}|$, implying massless excitations around the Dirac points, as in the case of graphene.

In contrast to the band structure, the normalized eigenvectors $\psi_{\mathbf{k},\lambda}$ depend on α and are given by

$$\psi_{\mathbf{k},\pm} = \frac{1}{\sqrt{2}}\begin{pmatrix} \mu\cos\phi e^{-i\mu\theta_\mathbf{k}} \\ \pm 1 \\ \mu\sin\phi e^{i\mu\theta_\mathbf{k}} \end{pmatrix}, \quad \psi_{\mathbf{k},0} = \begin{pmatrix} \sin\phi e^{-i\mu\theta_\mathbf{k}} \\ 0 \\ -\cos\phi e^{i\mu\theta_\mathbf{k}} \end{pmatrix},$$

where $\theta_\mathbf{k} = \tan^{-1}(k_y/k_x)$. Moreover, the elements of the spinors from top to bottom represent the probability amplitude of staying in sublattices A (rim), B (hub), and C (rim), respectively. The flat-band wave function exhibits that the probability amplitude of an electronic wave function centered over the hub sites is always zero. Hence, electrons in the flat band remain localized around the rim sites.

For $\alpha = 1$, Eq. (2) reduces to the pseudospin-1 Dirac-Weyl Hamiltonian $H_0^\mu(\mathbf{k}) = \hbar v_f \mathbf{S}\cdot\mathbf{k}$, where $\mathbf{S} = (S_x, S_y, S_z)$ are the standard spin-1 matrices.

Berry phase. The topological Berry phase for $\alpha = 0$ is simply π, which is independent of the valleys. For $\alpha > 0$, the α-dependent Berry phase [27] $\phi_B^{\lambda,\mu}$ in the conduction and valence bands is given by

$$\phi_B^{\pm 1,\mu} = \pi\mu\cos(2\phi) = \pi\mu\left(\frac{1-\alpha^2}{1+\alpha^2}\right), \tag{5}$$

and for the flat band is given by

$$\phi_B^{0,\mu} = -2\pi\mu\cos(2\phi) = -2\pi\mu\left(\frac{1-\alpha^2}{1+\alpha^2}\right). \tag{6}$$

Note that the Berry phase is different in the $\mathbf{K}$ and $\mathbf{K}'$ valleys, except for $\alpha = 1$. The Berry phase is smoothly decreasing with increase of α and becomes zero at $\alpha = 1$. Later, we will show how the Berry phase appears in quasienergy gaps.

III. FLOQUET EIGENSYSTEM FOR α-T_3 LATTICE

We consider a circularly polarized electromagnetic radiation propagating perpendicular to the α-T_3 lattice placed in the x-y plane. The corresponding vector potential is given by $\mathbf{A}(t) = A_0(\cos\omega t\,\hat{\mathbf{x}} + \nu \sin\omega t\,\hat{\mathbf{y}})$, where $A_0 = E_0/\omega$ in which E_0 is the amplitude of the electric field and ω is the frequency of the radiation. Also, $\nu = \pm 1$ denotes counterclockwise and clockwise rotations of the circularly polarized light, respectively. The frequency of the driving is small compared to the bandwidth of the system. The vector potential satisfies the time periodicity: $\mathbf{A}(t+T) = \mathbf{A}(t)$ with the time period $T = 2\pi/\omega$. The minimal coupling between the charge carrier and the electric field is obtained through the Peierls substitution: $\hbar\mathbf{k} \to [\hbar\mathbf{k} - q\mathbf{A}(t)]$, with $q = -e$ being the electronic charge. The Hamiltonian for the coupling between the charge carriers and the electromagnetic field can be written as

$$H_1^{\mu\nu}(t) = \hbar\omega\beta[S_-^{\mu\nu}e^{i\omega t} + S_+^{\mu\nu}e^{-i\omega t}], \tag{7}$$

where the 3×3 matrices are $S_\pm^{\mu\nu} = \frac{1}{2}[\mu S_x(\alpha) \pm i\nu S_y(\alpha)]$ and the dimensionless parameter $\beta = eE_0 l_\omega/(\hbar\omega)$ characterizes the strength of the coupling between the electromagnetic radiation and charge carrier with $l_\omega/a = 3\pi t/\hbar\omega \gg 1$ in the THz frequency regime. The dimensionless parameter β is less than 1 for the typical intensity of lasers available in the THz frequency regime. In the semiclassical picture, $eE_0 l_\omega$ is the energy gained by the charge carrier while traveling a distance l_ω with the speed v_f during one period of the radiation. On the other hand, the charge carrier is dressed with the minimal photon energy $\hbar\omega$.

The total Hamiltonian of a charge carrier near the Dirac point in the presence of the electromagnetic radiation is $H^{\mu\nu}(\mathbf{k},t) = H_0^{\mu}(\mathbf{k}) + H_1^{\mu\nu}(t)$, which is periodic in time. By Floquet theory, the solution of the time-dependent Schrodinger equation

$$i\hbar\frac{\partial}{\partial t}\left|\psi_\eta^{\mu\nu}(\mathbf{k},t)\right\rangle = H^{\mu\nu}(\mathbf{k},t)\left|\psi_\eta^{\mu\nu}(\mathbf{k},t)\right\rangle \tag{8}$$

is given by

$$\left|\psi_\eta^{\mu\nu}(\mathbf{k},t)\right\rangle = e^{-i\varepsilon_\eta^{\mu\nu}(\mathbf{k})t/\hbar}\left|\phi_\eta^{\mu\nu}(\mathbf{k},t)\right\rangle. \tag{9}$$

Here, $|\phi_\eta^{\mu\nu}(\mathbf{k},t)\rangle$ are the time-periodic 1×3 pseudospinors and $\varepsilon_\eta^{\mu\nu}(\mathbf{k})$ are the corresponding quasienergies. There are three independent quasienergy branches along with the three corresponding eigenstates indexed by $\eta = 1, 0, -1$. Substituting Eq. (9) into Eq. (8), the time-periodic spinor $|\phi_\eta^{\mu\nu}(\mathbf{k},t)\rangle$ becomes the eigenstate of the Floquet Hamiltonian $H_F^{\mu\nu} = H^{\mu\nu}(\mathbf{k},t) - i\hbar\frac{\partial}{\partial t}$ with the eigenvalue $\epsilon_\eta^{\mu\nu}(\mathbf{k})$:

$$\left[H^{\mu\nu}(\mathbf{k},t) - i\hbar\frac{\partial}{\partial t}\right]\left|\phi_\eta^{\mu\nu}(\mathbf{k},t)\right\rangle = \epsilon_\eta^{\mu\nu}(\mathbf{k})\left|\phi_\eta^{\mu\nu}(\mathbf{k},t)\right\rangle. \tag{10}$$

Multiplying a phase $e^{-im\omega t}$, with m being an integer to Eq. (9), and substituting it back to Eq. (10), we obtain

$$\left[H^{\mu\nu}(\mathbf{k},t) - i\hbar\frac{\partial}{\partial t}\right]\left|\phi_\eta^{\mu\nu}(\mathbf{k},t)\right\rangle = \left[\varepsilon_\eta^{\mu\nu}(\mathbf{k}) + m\hbar\omega\right]\left|\phi_\eta^{\mu\nu}(\mathbf{k},t)\right\rangle. \tag{11}$$

This is also an eigenvalue equation like Eq. (10), but with a shifted quasienergy $\varepsilon_{\eta m}^{\mu\nu}(\mathbf{k}) = \varepsilon_\eta^{\mu\nu}(\mathbf{k}) + m\hbar\omega$. Equations (10) and (11) yield the same Floquet mode, with quasienergies differing by an integer multiple of photon energy $\hbar\omega$. Hence, the index η corresponds to a whole class of solutions indexed by $\eta' = (\eta, m)$, $m = 0, \pm1, \pm2, \ldots$ having a discrete spectrum of quasienergies $\varepsilon_{\eta,m}(\mathbf{k})$. Thus, a given Floquet state has multiple quasienergy values repeating in the intervals of $\hbar\omega$. For the α-T_3 lattice, we have three independent values of quasienergy for a given momentum, which can be attributed to the three independent eigenvalue equations ($\eta = 1, 0, -1$). Due to the infinite spectrum without physical distinguishability, the quasienergies can also be confined to a reduced Brillouin zone in the energy space with $|\varepsilon_\eta^{\mu\nu}(\mathbf{k})| < \hbar\omega/2$.

In order to calculate the quasienergies and the corresponding states of the Floquet Hamiltonian, we consider the Fourier expansion of $|\phi_\eta^{\mu\nu}(\mathbf{k},t)\rangle$,

$$\left|\phi_\eta^{\mu\nu}(\mathbf{k},t)\right\rangle = \sum_{n=-\infty}^{\infty} e^{-in\omega t}\left|\chi_\eta^{n\mu\nu}(\mathbf{k})\right\rangle, \tag{12}$$

which follows from the temporal periodicity of the Floquet mode. Using Eq. (12), the time-dependent differential given by Eq. (10) reduces to the time-independent eigensystem problem as

$$\sum_m \left[H_{0F,mn}^{\mu\nu} + H_{1F,mn}^{\mu\nu} - \epsilon_\eta^{\mu\nu}(\mathbf{k})\right]\left|\chi_\eta^{m\mu\nu}(\mathbf{k})\right\rangle = 0, \tag{13}$$

where the diagonal Floquet Hamiltonian in the Floquet basis is

$$H_{0F,mn}^{\mu\nu} = [\hbar v_f \mathbf{S}(\alpha)\cdot\mathbf{k} + m\hbar\omega]\delta_{mn}, \tag{14}$$

and the off-diagonal interaction Hamiltonian

$$H_{1F,mn}^{\mu\nu} = \hbar\omega\beta[S_-^{\mu\nu}\delta_{m,n-1} + S_+^{\mu\nu}\delta_{m,n+1}] \tag{15}$$

couples various Fourier modes. Thus, by Floquet matrix theory, we numerically compute the Floquet quasienergies $\varepsilon_\eta^{\mu\nu}$ in units of $\hbar\omega$ and the corresponding Floquet states $|\psi_\eta^{\mu\nu}(k,t)\rangle$ of the Floquet Hamiltonian $H_F^{\mu\nu}$. The following parameters have been used in the numerical calculation: $\omega = 2\pi \times 5$ THz, $E_0 = 2$ kV/cm, $v_f = 10^6$ m/s, and $\beta = 0.3$. Also, $\mu = \nu = +1$ are considered for all the plots unless otherwise stated.

A. Exact analytical expressions of quasienergies and band gap at the Dirac points

First, we present exact analytical results of quasienergies and band gaps at the Dirac points. At the Dirac points ($\mathbf{k} = 0$), the time-dependent Hamiltonian (in units of $\hbar\omega$) can be written as

$$\bar{H}_1^{\mu\nu}(\tilde{t}) = \beta[S_-^{\mu\nu}e^{i\tilde{t}} + S_+^{\mu\nu}e^{-i\tilde{t}}], \tag{16}$$

where $\tilde{t} = \omega t$. The corresponding Floquet Hamiltonian can be written explicitly as

$$\tilde{H}_F^{\mu\nu}(\tilde{t}) = \mu\beta\begin{bmatrix} -i\frac{\partial}{\partial\tilde{t}} & \cos\phi e^{-i\mu\nu\tilde{t}} & 0 \\ \cos\phi e^{i\mu\nu\tilde{t}} & -i\frac{\partial}{\partial\tilde{t}} & \sin\phi e^{-i\mu\nu\tilde{t}} \\ 0 & \sin\phi e^{i\mu\nu\tilde{t}} & -i\frac{\partial}{\partial\tilde{t}} \end{bmatrix}. \tag{17}$$

Let us define a unitary operator $\hat{Q}$ given by

$$\hat{Q} = e^{-i\mu\nu(I+S_z)\tilde{t}}, \tag{18}$$

where I is the 3×3 identity matrix. By performing the unitary transformation $\hat{Q}^\dagger \tilde{H}_F^{\mu\nu}(\tilde{t})\hat{Q}$, an effective time-independent Floquet Hamiltonian is obtained:

$$\tilde{H}_F^{\mu\nu} = \mu \begin{bmatrix} -2\nu & \beta\cos\phi & 0 \\ \beta\cos\phi & -\nu & \beta\sin\phi \\ 0 & \beta\sin\phi & 0 \end{bmatrix}. \tag{19}$$

The zero-momentum quasienergy spectra are given by

$$\lambda_1 = -\mu\nu + \frac{2\mu}{\sqrt{3}}\sqrt{1+\beta^2}\cos\Lambda, \tag{20}$$

$$\lambda_2 = -\mu\nu - \frac{\mu}{3}\sqrt{1+\beta^2}(\sqrt{3}\cos\Lambda + 3\sin\Lambda), \tag{21}$$

$$\lambda_3 = -\mu\nu - \frac{\mu}{3}\sqrt{1+\beta^2}(\sqrt{3}\cos\Lambda - 3\sin\Lambda), \tag{22}$$

where $\Lambda = (1/3)\mathrm{Arg}[-\xi + \sqrt{\xi^2 - 108(1+\beta^2)^3}]$ and $\xi = 27\nu\beta^2(\frac{1-\alpha^2}{1+\alpha^2})$, with $\mathrm{Arg}[z]$ giving the argument of the complex number z. The corresponding normalized Floquet states are given by

$$|\psi^{\mu\nu}(\tilde{t})\rangle = \frac{e^{-i(\lambda_i+\mu\nu)\tilde{t}}}{\sqrt{1+\beta^2\left[\frac{\cos^2\phi}{(2\mu\nu+\lambda_i)^2} + \frac{\sin^2\phi}{\lambda_i^2}\right]}} \begin{pmatrix} \frac{\beta\cos\phi}{2\mu\nu+\lambda_i} e^{-i\mu\nu\tilde{t}} \\ 1 \\ \frac{\beta\sin\phi}{\lambda_i} e^{i\mu\nu\tilde{t}} \end{pmatrix}.$$

The parameter ξ can be expressed in terms of the Berry phase given by Eqs. (5) and (6). Thus, the quasienergy is directly related to the Berry phase acquired during a cyclic motion of the charge carriers in the presence of a circularly polarized radiation.

The three Floquet quasienergy branches may be labeled as (i, m), where $i = 1, 2, 3$ represent three branches and m the Floquet index. The corresponding quasienergy $\lambda_{i,m} = \lambda_i + m$. The quasienergies of the three branches in the first energy Brillouin zone (BZ) are given by $\lambda_1 + \mu(\nu - 1)$, $\lambda_2 + \mu(\nu + 1)$, and $\lambda_3 + \mu\nu$. The threefold degeneracy at the Dirac point is simply the limiting case ($\beta \to 0$) of these quasienergies. The variation of these quasienergies with α for $\beta = 0.3$ is shown in Fig. 2. Figure 2 displays the photoinduced valley and electron-hole symmetry breaking at the Dirac point for $0 < \alpha < 1$. The quasienergy variations for the pair having the same value of $\mu\nu$ (i.e., $\mu\nu = 1$ [Figs. 2(a) and 2(b)] or $\mu\nu = -1$ [Figs. 2(c) and 2(d)]) are identical to each other, apart from the interchange of branches. Also, the quasienergy structure for the cases of $\mu\nu = 1$ and $\mu\nu = -1$ are inverted copies of each other for $0 < \alpha < 1$. This implies that the spectrum undergoes a flipping on (i) switching between valleys **K** and **K**′ for a given sense of circular polarization and (ii) changing sense of rotation of the polarization for a given valley. The flipping of quasienergies is trivially symmetric for graphene ($\alpha = 0$) and a dice lattice ($\alpha = 1$) on switching of valleys or polarization.

For $\alpha = 0$, the quasienergies within the first energy BZ are obtained as

$$\lambda_\pm = \pm\tfrac{1}{2}(\sqrt{4\beta^2+1} - 1). \tag{23}$$

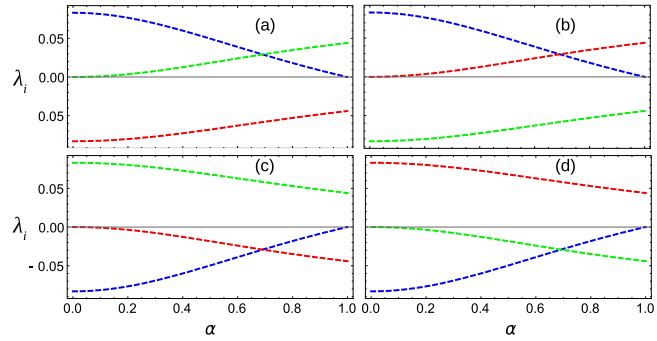

FIG. 2. Plots of quasienergies at the Dirac point vs α for various combinations of μ and ν: (a) $\mu = \nu = 1$, (b) $\mu = \nu = -1$, (c) $\mu = 1$, $\nu = -1$, (d) $\mu = -1$, $\nu = 1$. The green, red, and blue dotted curves correspond to λ_1, λ_2, and λ_3.

The same results are obtained by Oka and Aoki [6] for irradiated graphene. On the other hand, the quasienergies for the dice lattice ($\alpha = 1$) obtained from Eqs. (20)–(22) are $\lambda_0 = 0$ and

$$\lambda_\pm = \pm(\sqrt{\beta^2+1} - 1). \tag{24}$$

Equations (23) and (24) can be combined to write a general form for quasienergy at the Dirac point as

$$\lambda_\pm(S) = \pm(\sqrt{\beta^2+S^2} - S), \tag{25}$$

where S is the pseudospin of the underlying lattice. The energy gap at the Dirac point for the pseudospin S is $\Delta_S = \lambda_+(S) - \lambda_-(S) = 2(\sqrt{\beta^2+S^2} - S)$. The energy gap for graphene is $\Delta_{S=\frac{1}{2}} = (\sqrt{4\beta^2+1} - 1)$ and that for the dice lattice is $\Delta_{S=1} = 2(\sqrt{\beta^2+1} - 1)$. It can be easily checked from Fig. 3(a) as well as from Eq. (25) that $\Delta_{S=1} < \Delta_{S=\frac{1}{2}}$. The quasienergy gap at the Dirac point for graphene is higher than that of dice lattice. Thus, the flat band has a shielding effect on the dipole coupling between the electron-photon levels.

In Fig. 3, we show the variation of the three quasienergy branches with α and β. The color labeling of Fig. 3 is the same as that of Fig. 2(a). Figure 3(a) shows that our numerical results match very well with the exact results. The quasienergy at the Dirac point increases with the field strength β seen in Fig. 3(b).

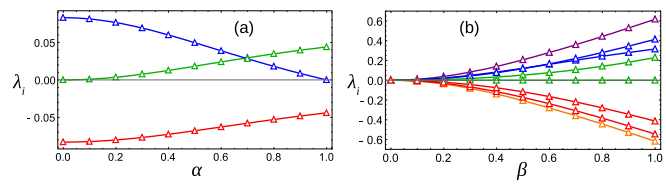

FIG. 3. Plots of variation of the exact quasienergy at the Dirac point with (a) α for $\beta = 0.3$ and (b) β for different values of α. Exact numerical results are denoted by the triangles. In (b), the solid green, blue, and red lines are for $\alpha = 1$, the dotted lines for $\alpha = 0.5$, and the purple-orange pair is for $\alpha = 0$.

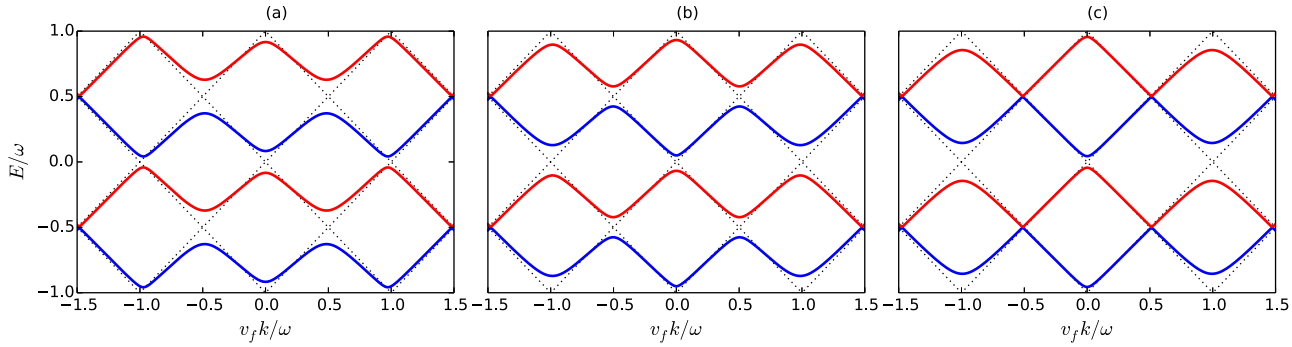

FIG. 4. Floquet quasienergy bands for different values of α: (a) $\alpha = 0$, (b) $\alpha = 0.5$, (c) $\alpha = 1$.

B. Floquet quasienergy branches and band gaps for large values of momentum

In this section, we present the results obtained by solving the low-energy Floquet Hamiltonian numerically and display the quasienergy band structure within the first two energy Brillouin zones in Fig. 4 for $\alpha = 0$, 0.5, and 1. The dotted lines indicate the spectrum for zero intensity of radiation, which are identical for all values of α. First of all, the quasienergies of the α-T_3 lattice pertaining to different η satisfy $\varepsilon_1^{\mu\nu}(\mathbf{k}) = -\varepsilon_{-1}^{\mu\nu}(\mathbf{k})$ for $\alpha = 0$, 1 and $\varepsilon_\eta^{\mu\nu}(\mathbf{k}) = \varepsilon_\eta^{\mu\nu}(-\mathbf{k})$ for $0 \leqslant \alpha \leqslant 1$. The known results of graphene ($\alpha = 0$) are reproduced in Fig. 4(a). For better visualization, the quasienergy band for $\eta = 0$ is shown separately in Fig. 5. The quasienergy branch corresponding to the flat band becomes dispersive mainly around the Dirac and even-photon resonant points for $0 < \alpha < 1$. This is due to the fact that the flat-band states are dressed with integral number of photons in the vicinity of these resonant points, which allows them to mix with dressed conduction- and valence-band states. The mixing results in dispersion due to shifting of energies of the erstwhile nondispersive states. On the other hand, the band does not undergo any significant modification at odd-photon resonances, as it cannot be dressed with a half-integral number of photons. The dispersion gets completely wiped out at $\alpha = 1$. The height of the spikes of the dispersion decreases with increases of the momentum. The band structure gets inverted about the k axis on changing the rotation of the electric-field vector of the circularly polarized light. The band remains flat for all values of α when applied radiation is linearly polarized. It is to be noted that there is no splitting in the flat band since it does not have any partner band.

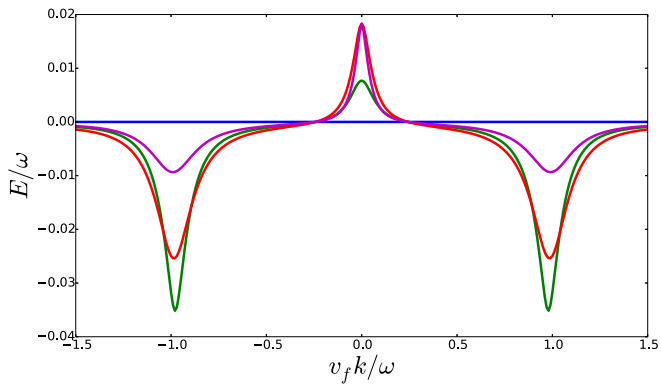

FIG. 5. Quasienergy band for $\eta = 0$ at different values of α: (i) $\alpha = 0.3$ (green), (ii) $\alpha = 0.5$ (red), (iii) $\alpha = 0.8$ (purple), and $\alpha = 1$ (blue).

The gaps between the bands ($\eta = \pm 1$) open up at $k = 0$ and at $k_m = m\omega/2v_f$ with $m = \pm 1, \pm 2, \ldots$. The gap at k_m arises due to the ac Stark splitting occurring due to the multiphoton resonances [12,44–48]. There is a set of Bloch states lying on a circle in the vicinity of the Dirac point k space with radius k_m such that the energy difference between the bands is m multiples of the photon energy: $2v_f k_m = m\omega$. On illumination, new electron-photon states with energy $E_\lambda = \hbar v_f k_m + N_\lambda \hbar\omega$ (λ band with N_λ photons) and $E_{\lambda'} = -\hbar v_f k_m + N_{\lambda'}\hbar\omega$ with $\lambda' \neq \lambda$ (λ' state with $N_{\lambda'}$ photons) are formed. When $E_\lambda = E_{\lambda'}$, i.e., $N_\lambda - N_{\lambda'} = m\hbar\omega$, the degenerate levels split due to the coupling between the electron and the radiation field and the gap opens up at k_m. All the gaps tend to diminish at higher values of momentum.

Using the rotating wave approximation (see the Appendix), the approximate quasienergies for $\alpha = 0$ (for any integer m) and $\alpha = 1$ (for even m) are, respectively, given by

$$(\lambda_\pm)_{\alpha=0} = \pm\frac{\beta}{2}|J_{m+1}(2\beta) - J_{m-1}(2\beta)|, \tag{26}$$

$$(\lambda_\pm)_{\alpha=1} = \pm\frac{\beta}{2}|J_{m/2+1}(\beta) - J_{m/2-1}(\beta)|. \tag{27}$$

From the above expressions, we can see that $(\lambda_\pm)_{\alpha=0}$ and $(\lambda_\pm)_{\alpha=1}$ are proportional to the difference between two consecutive integral and even-ordered Bessel functions, respectively. The magnitude of the gaps is strongly affected by the argument of the Bessel functions which, for graphene, is twice that of the dice lattice. For $\beta \ll 1$, the asymptotic forms of the quasienergy gaps are $(\Delta_m)_{\alpha=0} \sim \beta^m$ and $(\Delta_m)_{\alpha=1} \sim (\beta/2)^{m/2}$. For weak fields, $(\Delta_1)_{\alpha=0}$ and $(\Delta_2)_{\alpha=1}$ vary linearly with β. The variation of the gaps Δ_m with β and α are shown in Figs. 6 and 7, respectively. The curves represent the numerical results, while their corresponding markers represent the results obtained from the exact analytical expressions (Δ_0) and rotating wave approximation (Δ_1, Δ_2, Δ_3). All the gaps increase monotonically with β. Moreover, Δ_0 (solid blue) and Δ_1 (dashed purple) get reduced at higher α. In contrast, Δ_2 (dotted red) is found to increase with α. The gap Δ_3 (dash-dotted green) increases very slowly with α. The splitting at even-photon resonant points is affected by the intervention of the flat band dressed with an integral number of photons. The

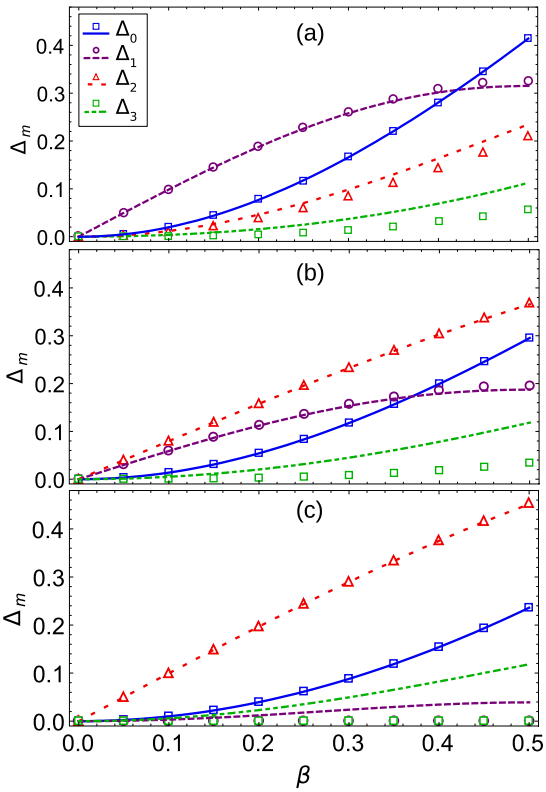

FIG. 6. Plots of variation of gaps Δ_m with β for (a) $\alpha = 0$, (b) $\alpha = 0.5$, and (c) $\alpha = 1$.

interplay of the three bands results in an increase in magnitude of the gap as α increases. We see that the agreement between numerical and analytical results does not hold well at higher momentum.

IV. TIME-AVERAGED ENERGIES AND DENSITY OF STATES

In this section, we discuss time-averaged quantities such as mean energy and the corresponding density of states. The mean energy is a single-valued quantity, which is independent of the choice of the quasienergy of the Floquet state. The mean energy helps one to understand whether the Floquet states are occupied or unoccupied [12,46,47]. For example, the Floquet states having lower mean quasienergy will be accommodated

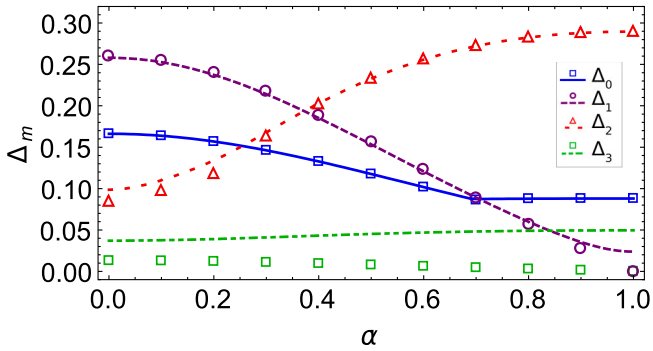

FIG. 7. Plots of variation of gaps Δ_m with α for $\beta = 0.3$.

first. Also, the mean quasienergy can be used to characterize whether the state is electronlike or holelike [10].

Time-averaged energies. The expectation value of the Hamiltonian in a Floquet state is a periodic function of time. This helps us to formulate the energy averaged over a full cycle of a periodic driving and is given by

$$E_\eta^{\bar{\mu}\nu}(\mathbf{k}) = \frac{1}{T}\int_0^T \langle \psi_\eta^{\mu\nu}(\mathbf{k},t)|H^{\mu\nu}(\mathbf{k},t)|\psi_\eta^{\mu\nu}(\mathbf{k},t)\rangle dt. \quad (28)$$

Incorporating the Fourier series [Eq. (12)] into the above equation, we get

$$\bar{E}_\eta^{\mu\nu}(\mathbf{k}) = \varepsilon_\eta^{\mu\nu}(\mathbf{k}) + \sum_{n=-\infty}^{\infty} n\hbar\omega\langle\chi_\eta^{n\mu\nu}(\mathbf{k})|\chi_\eta^{n\mu}(\mathbf{k})\rangle. \quad (29)$$

Hence, the averaged energy can be viewed as the weighted average of energies possessed by the Fourier harmonics of the Floquet modes.

The time-averaged energy (around the **K** valley) corresponding to the Floquet states of the three branches for different values of α is shown in Fig. 8. The blue, green, and red bands represent the quasielectron, flat band, and quasihole states, respectively. For $0 < \alpha < 1$, the mean energy-band structure around $\mathbf{K}'$ can be obtained by simply inverting the same for the **K** valley. Due to the absence of inversion symmetry of the band structure for $0 < \alpha < 1$, the valley degeneracy is broken. As $\beta \to 0$, we obtain the field-free Dirac cones shown by the dotted lines. For $0 \leqslant \alpha < 1$, the mean energy goes to zero near one-photon and two-photon resonant points due to crossover between quasielectron and quasihole states [10]. The vanishing of mean energies at these resonant points is also observed for $\alpha < 1$. But, the dice lattice has a nonzero mean energy near *one-photon* resonance. This can be attributed to the fact that the gap at *one-photon* resonance becomes vanishingly small and mimics the radiation-free case for $\alpha = 1$. A finite gap exists at the Dirac point for all values of α. The threefold degeneracy at the Dirac point is lifted by the radiation. Careful examination reveals that the symmetric nature of the $\eta = \pm 1$ bands (electron-hole symmetry) is slightly disrupted near the Dirac point for $0 < \alpha < 1$. The symmetry is restored at $\alpha = 1$. A distortion occurs in the mean energy spectrum of the flat band at $k = 0, \pm\omega/v_f$, similar to that obtained in the quasienergy spectrum. The distortions flatten out at $\alpha = 1$.

Time-averaged density of states. The time-averaged density of states over a driving cycle is defined as

$$D(E) = g_s \sum_{n,\eta,\mu,\mathbf{k}} \langle\chi_\eta^n(\mathbf{k})|\chi_\eta^n(\mathbf{k})\rangle\delta\{E - [\varepsilon_\eta(\mathbf{k}) + n\hbar\omega]\}. \quad (30)$$

Here, the factor $g_s = 2$ appears due to the spin degeneracy. On converting the sum over $\mathbf{k}$ to integral, i.e., $\sum_{\mathbf{k}} \to \frac{1}{(2\pi)^2}\int^{\mathbf{k}} d^2\mathbf{k}$, and using the azimuthal symmetry of the quasienergy band structure for circularly polarized light, we get the density of states per unit area as

$$g(E) = D_0 \sum_{\eta,n,\mu} \int_0^\infty \langle\chi_\eta^{n\mu}(\tilde{k})|\chi_\eta^{n\mu}(\tilde{k})\rangle \times \delta\{\tilde{\varepsilon} - [\tilde{\varepsilon}_\eta^\mu(\tilde{k}) + n]\}\tilde{k}d\tilde{k}, \quad (31)$$

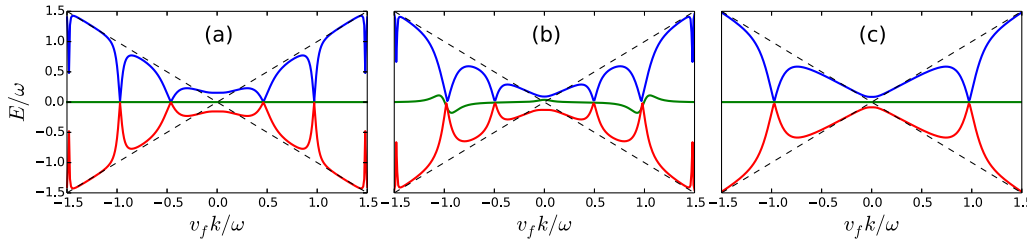

FIG. 8. Time-averaged energy of the three Floquet branches for (a) $\alpha = 0$, (b) $\alpha = 0.5$, (c) $\alpha = 1$.

where $D_0 = g_s\omega/(2\pi\hbar v_f^2) = 1.515 \times 10^{13}$ meV^{-1} m^{-2}. $\tilde{\varepsilon}$ and $\tilde{\varepsilon}_\eta^\mu(\tilde{k})$ are the dimensionless quasienergies such that $E = \tilde{\varepsilon}\hbar\omega$. Using the property of the Dirac δ function, the above integral can be further simplified as

$$g(E) = D_0 \sum_{\gamma,\tilde{k}_i^{(\gamma)}(\tilde{\varepsilon})} \frac{\langle \chi_\eta^{n\mu}(\tilde{k}_i^{(\gamma)}(\tilde{\varepsilon}))|\chi_\eta^{n\mu}(\tilde{k}_i^{(\gamma)}(\tilde{\varepsilon}))\rangle \tilde{k}_i^{(\gamma)}(\tilde{\varepsilon})}{|\tilde{\varepsilon}'_\eta(\tilde{k}_i^{(\gamma)}\tilde{\varepsilon})|}, \quad (32)$$

where $\gamma = \{n, \eta, \mu\}$ is a set of quantum numbers and $\tilde{k}_i^{(\gamma)}(\tilde{\varepsilon})$ is the ith positive root of $\tilde{\varepsilon} - [\tilde{\varepsilon}_\eta^\mu(\tilde{k}) + n] = 0$ for a given n.

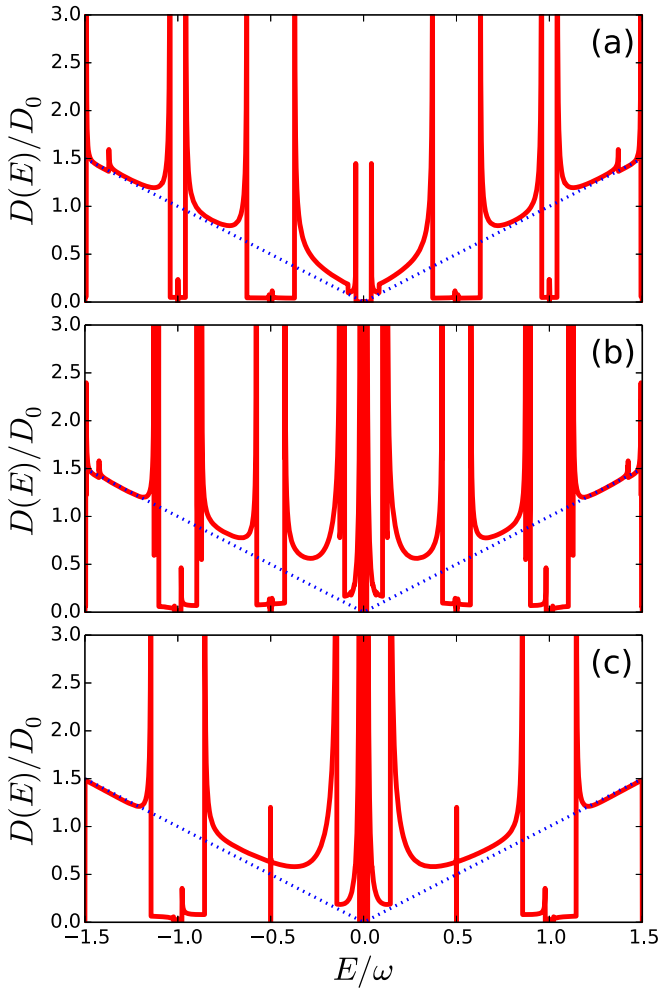

FIG. 9. Time-averaged density of states of quasielectron and quasihole states for (a) $\alpha = 0$, (b) $\alpha = 0.5$, (c) $\alpha = 1$.

The time-averaged density of states of electronlike and holelike quasienergy bands for three different values of α is shown in Fig. 9. Figure 9(a) shows the DOS for $\alpha = 0$, which is similar to the results obtained by other groups [6,10]. The peaks represent the van Hove singularities occurring due to the extrema in the quasienergy band structure. Apart from large peaks, there are spikes around $E = \pm\omega/2$ and $E = \pm\omega$ with vanishingly small DOS. This is because of the photoinduced gaps at the boundaries of the energy Brillouin zones. A small but finite contribution of DOS in these energy ranges appears due to closing of gaps at higher momenta. Additional peaks are born at the Dirac point for finite $0 < \alpha \leqslant 1$, as seen in Figs. 9(b) and 9(c). The separation between the peaks centered around $E = \pm\omega/2$ decreases with α, while that around $E = \pm\omega$ increases with α. This is related to the fact that $\Delta_1(\Delta_2)$ decreases (increases) with α.

The time-averaged DOS for the flat-band quasienergy around the Dirac point is shown in Fig. 10. Since the regions between two consecutive even-photon resonant points are predominantly flat, a large peak appears at zero energy. The dispersion at even-photon resonant points in the flat band lead to the occurrence of additional peaks symmetrically placed around around the peak at zero energy. A similar feature in the DOS is repeated at energies equal to integral multiples of photon energy. In the dice lattice, only central peaks are present at $N\hbar\omega$ (N being the integer) due to the absence of dispersion in the flat band.

V. SUMMARY AND CONCLUSION

We have investigated the Floquet quasienergy spectrum numerically and analytically for the α-T_3 lattice driven by circularly polarized radiation. Exact analytical expressions of

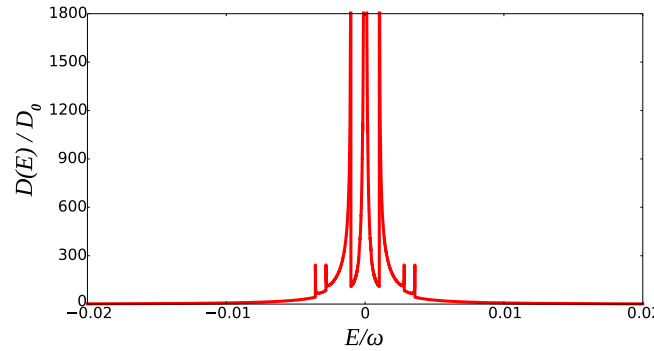

FIG. 10. Time-averaged density of states of quasiflat band around the Dirac point for $\alpha = 0.5$.

the quasienergy at the Dirac points for all values of α and field strength are provided. The band gap at the Dirac point appears due to the circularly polarized radiation for all values of α. The quasienergy gap at the Dirac point decreases with the increase of α. Within the rotating wave approximation, we are able to get approximate expressions of quasienergy at single-photon and multiphoton resonant points. Approximate results match very well with the numerical results based on the Floquet method. The expressions reveal that the quasienergy is directly related to the Berry phase acquired during a cyclic motion driven by the rotating electric field. The valley symmetry is broken due to the different Berry phase for different valleys for $0 < \alpha < 1$. The quasienergy flat band remains dispersionless in the presence of radiation for the dice lattice. However, dispersive spikes appear in and around the Dirac and even-photon resonant points for $0 < \alpha < 1$. The mean energy is nonvanishing around the single-photon resonance point for the dice lattice, unlike $\alpha < 1$. In contrast to graphene, we find that additional peaks appear in the time-averaged density of states at the Dirac point for $0 < \alpha \leqslant 1$. The pattern of the DOS near the single-photon and two-photon resonant points varies significantly with α.

Floquet-Bloch states on the surface of a topological insulator have been observed using time- and angle-resolved photoemission spectroscopy (TrARPES) [49]. There is a possibility that the quasienergy band structure of the α-T_3 lattice may be probed using TrARPES on subjecting the lattice to intense microwave pulses perpendicular to the lattice plane. The variation in quasienergy band gaps with α may be observed by modulating the phase of one of the three counterpropagating laser beams. Similarly, the quasienergy band structure for $\alpha = 1/\sqrt{3}$ may be verified by devising a suitable means to irradiate $Hg_{1-x}Cd_xTe$ quantum wells. The radiation-dressed band structure of such systems may open up doors for new optoelectronic devices.

ACKNOWLEDGMENTS

We would like to thank Firoz Islam and Sonu Verma for useful discussions.

APPENDIX: ANALYTICAL RESULTS WITHIN ROTATING WAVE APPROXIMATION

In this Appendix, we shall derive analytical expressions of the quasienergy branches within the rotating wave approximation [10]. The analytical expressions help us to understand the Berry phase dependency of the quasienergy bands and band gaps.

The time-periodic Hamiltonian $H^{\mu\nu}(\mathbf{k}, t)$ can be transformed in the basis formed by the eigenvectors of the low-energy Hamiltonian $H_0^{\mu}(\mathbf{k})$ with the help of the unitary operator $\hat{U}_{\mathbf{k}}$ given by

$$\hat{U}_{\mathbf{k}} = \frac{1}{\sqrt{2}} \begin{pmatrix} \mu\cos\phi e^{-i\mu\theta_{\mathbf{k}}} & \sqrt{2}\sin\phi e^{-i\mu\theta_{\mathbf{k}}} & \mu\cos\phi e^{-i\mu\theta_{\mathbf{k}}} \\ 1 & 0 & -1 \\ \mu\sin\phi e^{i\mu\theta_{\mathbf{k}}} & -\sqrt{2}\cos\phi e^{i\mu\theta_{\mathbf{k}}} & \sin\phi e^{i\mu\theta_{\mathbf{k}}} \end{pmatrix}.$$

The transformed Hamiltonian $\hat{U}_{\mathbf{k}}^{\dagger} H^{\mu\nu}(\mathbf{k}, t)\hat{U}_{\mathbf{k}} = \tilde{H}^{\mu\nu}(\mathbf{k}, t)$ reads

$$\tilde{H}^{\mu\nu}(\mathbf{k}, t) = \hbar\omega\left[\frac{v_f k}{\omega} S_z + \tilde{H}_{\text{intra}}(t) + \tilde{H}_{\text{inter}}(t)\right], \tag{A1}$$

where $\tilde{H}_{\text{intra}}(t) = \beta(\cos\mu\theta_k \cos\omega t + \mu\nu \sin\mu\theta_k \sin\omega t)S_z$, with S_z being the z component of the spin-1 matrix and

$$\tilde{H}_{\text{inter}}(t) = \frac{if(t)}{\sqrt{2}} \begin{bmatrix} 0 & \sin 2\phi & \sqrt{2}\mu\cos 2\phi \\ -\sin 2\phi & 0 & \sin 2\phi \\ -\sqrt{2}\mu\cos 2\phi & -\sin 2\phi & 0 \end{bmatrix}, \tag{A2}$$

where $f(t) = \beta(\nu\cos\mu\theta_k \sin\omega t - \mu\sin\mu\theta_k \cos\omega t)$.

The Schrodinger equation is then given by

$$\left\{\frac{i}{\omega}\partial_t - \left[\frac{v_f k}{\omega} S_z + \tilde{H}_{\text{intra}}(t) + \tilde{H}_{\text{inter}}(t)\right]\right\} |\psi_\eta(\mathbf{k}, t)\rangle = 0. \tag{A3}$$

We solve the Schrodinger equation by omitting the interband term $\tilde{H}_{\text{inter}}(t)$ and get the following solutions:

$$\begin{aligned} \left|\psi_{+1}^{(0)}(\mathbf{k}, t)\right\rangle &= e^{-iv_f kt} u(\theta_{\mathbf{k}}, t) \begin{pmatrix} 1 \\ 0 \\ 0 \end{pmatrix}, \\ \left|\psi_{-1}^{(0)}(\mathbf{k}, t)\right\rangle &= e^{iv_f kt} u^*(\theta_{\mathbf{k}}, t) \begin{pmatrix} 0 \\ 0 \\ 1 \end{pmatrix}, \\ \left|\psi_{0}^{(0)}(\mathbf{k}, t)\right\rangle &= \begin{pmatrix} 0 \\ 1 \\ 0 \end{pmatrix}, \end{aligned} \tag{A4}$$

where $u(\theta_{\mathbf{k}}, t) = \exp\{i\beta[-\cos\mu\theta_{\mathbf{k}} \sin\omega t + \mu\nu \sin\mu\theta_{\mathbf{k}} (\cos\omega t - 1)]\}$. Note that $u(\theta_{\mathbf{k}}, t)$ is also a time-periodic function. The quasienergy of $\psi_{(\mathbf{k},\eta)}^{(0)}(t)$ is exactly the same as the zero-field case. It tells us that all the quasienergy gaps appear due to the interband term $\tilde{H}_{\text{inter}}(t)$.

Let the solution of Eq. (A3) be of the form

$$|\psi_\eta(\mathbf{k}, t)\rangle = \sum_{\gamma=-1}^{1} a_{\eta,\gamma}(t)\left|\psi_\gamma^{(0)}(\mathbf{k}, t)\right\rangle.$$

We get

$$\partial_t a_{\eta,1}(t) = \frac{\omega}{\sqrt{2}}\{\sqrt{2}\mu\cos 2\phi\ a_{\eta,-1}(t)e^{2iv_f kt}[u^*(\theta_{\mathbf{k}}, t)]^2 + \sin 2\phi\ e^{iv_f kt} u^*(\theta_{\mathbf{k}}, t)a_{\eta,0}(t)\} f(t), \tag{A5}$$

$$\partial_{\bar{t}} a_{\eta,0}(t) = \frac{\omega}{\sqrt{2}}[-a_{\eta,1}(t)e^{-iv_f kt} u(\theta_{\mathbf{k}}, t) + a_{\eta,-1}(t)e^{iv_f kt} u^*(\theta_{\mathbf{k}}, t)] \sin 2\phi\ f(t), \tag{A6}$$

$$\partial_{\bar{t}} a_{\eta,-1}(t) = -\frac{\omega}{\sqrt{2}}\{\sqrt{2}\mu\cos 2\phi\ a_{\eta,1}(t)e^{-2iv_f kt}[u(\theta_{\mathbf{k}}, t)]^2 + \sin 2\phi\ e^{-iv_f kt} u(\theta_{\mathbf{k}}, t)a_{\eta,0}(t)\} f(t). \tag{A7}$$

Taking $(\beta\omega/\sqrt{2})y_l(\theta_k)$ and $(\beta\omega/\sqrt{2})z_l(\theta_k)$ as the discrete Fourier transform of the periodic functions $[u(\theta_{\mathbf{k}},t)]^2 f(t)$ and $u(\theta_{\mathbf{k}},t)f(t)$, respectively, we have

$$\partial_t a_{\eta,1}(t) = \frac{\beta\omega}{2}\left[\sqrt{2}\cos 2\phi\ a_{\eta,-1}(t)\sum_{l=-\infty}^{\infty} y_l^*(\theta_k)e^{i(2v_fk-l\omega)t} + \sin 2\phi\ a_{\eta,0}(t)\sum_{l=-\infty}^{\infty} z_l^*(\theta_k)e^{i(v_fk-l\omega)t}\right], \tag{A8}$$

$$\partial_t a_{\eta,0}(t) = \frac{\beta\omega}{2}\left[-a_{\eta,1}(t)\sum_{l=-\infty}^{\infty} z_l(\theta_k)e^{-i(v_fk-l\omega)t} + a_{\eta,-1}(t)\sum_{l=-\infty}^{\infty} z_l^*(\theta_k)e^{i(v_fk-l\omega)t}\right]\sin 2\phi, \tag{A9}$$

$$\partial_t a_{\eta,-1}(t) = -\frac{\beta\omega}{2}\left[\sqrt{2}\cos 2\phi\ a_{\eta,1}(t)\sum_{l=-\infty}^{\infty} y_l(\theta_k)e^{-i(2v_fk-l\omega)t} + \sin 2\phi\ a_{\eta,0}(t)\sum_{l=-\infty}^{\infty} z_l(\theta_k)e^{-i(v_fk-l\omega)t}\right]. \tag{A10}$$

Here,

$$z_l(\theta_k) = \frac{1}{\sqrt{2}}\big[u_{l+1}^{(1)}(\theta_k)(-\mu\sin\mu\theta_k + i\nu\cos\mu\theta_k) - u_{l-1}^{(1)}(\theta_k)(\mu\sin\mu\theta_k + i\nu\cos\mu\theta_k)\big] \tag{A11}$$

and

$$y_l(\theta_k) = \frac{1}{\sqrt{2}}\big[u_{l+1}^{(2)}(\theta_k)(-\mu\sin\mu\theta_k + i\nu\cos\mu\theta_k) - u_{l-1}^{(2)}(\theta_k)(\mu\sin\mu\theta_k + i\nu\cos\mu\theta_k)\big], \tag{A12}$$

where $u_l^{(j)}(\theta_k)$ with $(j=1,2)$ is defined as

$$u_l^{(j)}(\theta_k) = \frac{1}{T}\int_0^T [u(\theta_{\mathbf{k}},t)]^j e^{-il\omega t}dt. \tag{A13}$$

The exact expressions of $u_l^{(1)}(\theta_k)$ and $u_l^{(2)}(\theta_k)$ are obtained as

$$u_l^{(1)}(\theta_k) = e^{-i\mu\nu\beta\sin\mu\theta_k}J_l(2|p(\theta_k)|)\left[\frac{-p(\theta_k)}{|p(\theta_k)|}\right]^l, \tag{A14}$$

$$u_l^{(2)}(\theta_k) = e^{-i2\mu\nu\beta\sin\mu\theta_k}J_l(2|q(\theta_k)|)\left[\frac{-q(\theta_k)}{|q(\theta_k)|}\right]^l, \tag{A15}$$

where $J_l(x)$ is the lth-order Bessel function, $p(\theta_k) = \frac{\beta}{2}(\cos\mu\theta_k - i\mu\nu\sin\mu\theta_k)$, and $q(\theta_k) = \beta(\cos\mu\theta_k - i\mu\nu\sin\mu\theta_k)$. It is not possible to solve Eqs. (A8)–(A10) in closed analytical form. However, owing to the high frequency of the radiation, the standard rotating wave approximation (RWA) can be used to obtain closed-form expressions.

There are two frequency detuning terms, namely, $\delta_1 = 2v_fk - m\omega$ and $\delta_2 = v_fk - m\omega$, due to the presence of an additional dispersionless band. Near the resonance points, $(\delta_{1,2} \simeq 0)$, the momentum values k_m are such that the energy difference between the bands equals m multiples of photon energy $\hbar\omega$.

For even m (excluding 0), the terms $y_m(\theta_k)$ and $z_{m/2}(\theta_k)$ are retained in their respective series. But, for odd-integer m, we see that retaining the mth term from the $y_l(\theta_k)$ series allots v_fk/ω an odd-integer value. So within RWA, all the terms in the $z_l(\theta_k)$ series will be rapidly oscillating, allowing us to discard this series altogether. Hence, for odd m, we retain only $y_m(\theta_k)$. This leads to two distinct cases for even and odd integers, each of which produces separate systems of coupled differential equations for the determination of Floquet quasienergies.

Case I. For the even-m case, Eqs. (A8)–(A10) become

$$\partial_t a_{\eta,1}(t) = \frac{\beta\omega}{2}[\sqrt{2}\mu\cos 2\phi\ a_{\eta,-1}(t)y_m^*(\theta_k)e^{i\delta_1 t} + \sin 2\phi\ a_{\eta,0}(t)z_{m/2}^*(\theta_k)e^{i\delta_2 t}], \tag{A16}$$

$$\partial_t a_{\eta,0}(t) = \frac{\beta\omega}{2}[-a_{\eta,1}(t)z_{m/2}(\theta_k)e^{-i\delta_2 t} + a_{\eta,-1}(t)z_{m/2}^*(\theta_k)e^{i\delta_2 t}]\sin 2\phi, \tag{A17}$$

$$\partial_t a_{\eta,-1}(t) = -\frac{\beta\omega}{2}[\sqrt{2}\mu\cos 2\phi\ a_{\eta,1}(t)y_m(\theta_k)e^{-i\delta_1 t} + \sin 2\phi\ a_{\eta,0}(t)z_{m/2}(\theta_k)e^{-i\delta_2 t}]. \tag{A18}$$

Note that Eq. (A17) is redundant for the $\alpha = 0$ case. Equations (A16) and (A18) with $\alpha = 0$ reproduce all the approximate analytical results for graphene provided by Zhou and Wu [10].

Furthermore, the above set of equations cannot be solved analytically unless we solve it on exact resonance, i.e., $\delta_1 = \delta_2 = 0$. On exact resonance condition, the approximate expressions of the quasienergies for $0 < \alpha < 1$ obtained from Eqs. (A16)–(A18) are $\lambda_0 = 0$ and

$$\lambda_\pm = \pm\frac{\beta}{\sqrt{2}}\sqrt{\cos^2 2\phi|y_m(\theta_{\mathbf{k}})|^2 + \sin^2 2\phi|z_{m/2}(\theta_{\mathbf{k}})|^2}. \tag{A19}$$

From the above expression, we see that the quasienergy is proportional to the root mean modulus squared of the coupling parameters $y_m(\theta_{\mathbf{k}})$ and $z_{m/2}(\theta_{\mathbf{k}})$ weighted by terms dependent on the Berry phase ($\sim\cos 2\phi$) of the system. The sum of the weights is unity for all α. Since the Berry phase varies smoothly from π to 0 as α goes 0 to 1, the weight of $y_m(\theta_{\mathbf{k}})$ decreases while that of $z_{m/2}(\theta_{\mathbf{k}})$ increases with α. The quasieigenenergy for special cases such as $\alpha = 0$ and $\alpha = 1$ can be obtained easily. For $\alpha = 0$, $\lambda_\pm = \pm\frac{\beta}{\sqrt{2}}|y_m(\theta_{\mathbf{k}})|$. This is the same result as obtained for monolayer graphene [10]. On the other hand, for the dice lattice ($\alpha = 1$), we get $\lambda_\pm = \pm\frac{\beta}{\sqrt{2}}|z_{m/2}(\theta_{\mathbf{k}})|$ and $\lambda_0 = 0$. For the dice lattice, the quasienergy gap between $\eta = \pm 1$ at the resonance point is

$$\Delta_m(\theta_{\mathbf{k}}) = \sqrt{2}\beta|z_{m/2}(\theta_{\mathbf{k}})|. \tag{A20}$$

The magnitude of the gap in graphene and the dice lattice depends on the effective coupling parameters $|y_m(\theta_{\mathbf{k}})|$ and $|z_{m/2}(\theta_{\mathbf{k}})|$, respectively. The behavior of the gap in graphene and the dice lattice is quite different.

Case II. For the odd-m case, Eqs. (A8)–(A10) can be approximated as

$$\partial_t a_{\eta,1}(t) \approx \frac{\beta\omega\mu}{\sqrt{2}} \cos 2\phi \; a_{\eta,-1}(t) y_m^*(\theta_k) e^{i\delta_1 t}, \quad \text{(A21)}$$

$$\partial_t a_{\eta,0}(t) \approx 0, \quad \text{(A22)}$$

$$\partial_t a_{\eta,-1}(t) \approx -\frac{\beta\omega\mu}{\sqrt{2}} \cos 2\phi \; a_{\eta,1}(t) y_m(\theta_k) e^{-i\delta_1 t}. \quad \text{(A23)}$$

Thus, for odd m, we obtain a simplified expression of quasienergy for a given α,

$$\lambda_\pm \approx \pm\frac{\beta}{\sqrt{2}} |y_m(\theta_{\mathbf{k}})| \left(\frac{1-\alpha^2}{1+\alpha^2}\right), \quad \text{(A24)}$$

and $\lambda_0 = 0$. Interestingly, it shows that the gap with odd values of m closes in the dice lattice, which is in sharp contrast with the graphene case. Although Eq. (A24) shows that $\Delta_m = 0$ for $\alpha = 1$, this is not the case. We will get a small nonzero value of Δ_m on taking into account the higher-order contribution from Eqs. (A8)–(A10).

The quasienergy gap is essentially determined by the Berry phase and two coupling parameters $|y_m(\theta_{\mathbf{k}})|$ and $|z_{m/2}(\theta_{\mathbf{k}})|$. The expressions of the coupling parameters can be simplified further by setting $\theta_{\mathbf{k}} = 0$ since the quasienergy spectrum is isotropic for all values of α for circularly polarized light. On substitution of $\theta_{\mathbf{k}} = 0$ into Eqs. (A11) and (A12), we get

$$y_l(0) = \frac{iv}{\sqrt{2}}(-1)^l [J_{l-1}(2\beta) - J_{l+1}(2\beta)], \quad \text{(A25)}$$

$$z_l(0) = \frac{iv}{\sqrt{2}}(-1)^l [J_{l-1}(\beta) - J_{l+1}(\beta)]. \quad \text{(A26)}$$

Thus, the approximate forms of the quasienergies for $\alpha = 0$ (for any integer m) and $\alpha = 1$ (for even m) turn out to be

$$(\lambda_\pm)_{\alpha=0} = \pm\frac{\beta}{2} |J_{m+1}(2\beta) - J_{m-1}(2\beta)|, \quad \text{(A27)}$$

$$(\lambda_\pm)_{\alpha=1} = \pm\frac{\beta}{2} |J_{m/2+1}(\beta) - J_{m/2-1}(\beta)|. \quad \text{(A28)}$$

For the weak field ($\beta \ll 1$), the asymptotic forms of the quasienergy gaps are obtained from the above expressions as

$$(\Delta_m)_{\alpha=0} \sim \frac{\beta^m}{(m-1)!} \quad \text{and} \quad (\Delta_m)_{\alpha=1} \sim \frac{2(\beta/2)^{m/2}}{(m/2-1)!}. \quad \text{(A29)}$$

[1] P. Hanggi, *Quantum Transport and Dissipation* (Wiley, New York, 1988), Chap. 5.
[2] A. Eckardt and E. Anisimova, New J. Phys. **17**, 093039 (2015).
[3] M. V. Fistul and K. B. Efetov, Phys. Rev. Lett. **98**, 256803 (2007).
[4] S. V. Syzranov, M. V. Fistul, and K. B. Efetov, Phys. Rev. B **78**, 045407 (2008).
[5] F. J. Lopez-Rodriguez and G. G. Naumis, Phys. Rev. B **78**, 201406(R) (2008).
[6] T. Oka and H. Aoki, Phys. Rev. B **79**, 081406(R) (2009).
[7] T. Oka and H. Aoki, J. Phys.: Conf. Ser. **200**, 062017 (2010).
[8] W. Zhang, P. Zhang, S. Duan, and Xian-geng Zhao, New J. Phys. **11**, 063032 (2009).
[9] O. V. Kibis, Phys. Rev. B **81**, 165433 (2010).
[10] Y. Zhou and M. W. Wu, Phys. Rev. B **83**, 245436 (2011).
[11] A. Schloz, A. López, and J. Schliemann, Phys. Rev. B **88**, 045118 (2013).
[12] A. K. Gupta, O. E. Alon, and N. Moiseyev, Phys. Rev. B **68**, 205101 (2003).
[13] M. Ezawa, Phys. Rev. Lett. **110**, 026603 (2013).
[14] A. Lopez, A. Scholz, B. Santos, and J. Schliemann, Phys. Rev. B **91**, 125105 (2015).
[15] M. I. Katsnelson, *Graphene: Carbon in Two Dimensions* (Cambridge University Press, Cambridge, 2012).
[16] B. Sutherland, Phys. Rev. B **34**, 5208 (1986).
[17] J. Vidal, R. Mosseri, and B. Doucot, Phys. Rev. Lett. **81**, 5888 (1998).
[18] S. E. Korshunov, Phys. Rev. B **63**, 134503 (2001).
[19] M. Rizzi, V. Cataudella, and R. Fazio, Phys. Rev. B **73**, 144511 (2006).
[20] D. F. Urban, D. Bercioux, M. Wimmer, and W. Häusler, Phys. Rev. B **84**, 115136 (2011).
[21] J. D. Malcolm and E. J. Nicol, Phys. Rev. B **93**, 165433 (2016).
[22] D. Bercioux, D. F. Urban, H. Grabert, and W. Hausler, Phys. Rev. A **80**, 063603 (2009).
[23] M. Vigh, L. Oroszlány, S. Vajna, P. San-Jose, G. Dávid, J. Cserti, and B. Dóra, Phys. Rev. B **88**, 161413(R) (2013).
[24] F. Wang and Y. Ran, Phys. Rev. B **84**, 241103 (2011).
[25] A. Raoux, M. Morigi, J.-N. Fuchs, F. Piechon, and G. Montambaux, Phys. Rev. Lett. **112**, 026402 (2014).
[26] J. D. Malcolm and E. J. Nicol, Phys. Rev. B **92**, 035118 (2015).
[27] E. Illes, J. P. Carbotte, and E. J. Nicol, Phys. Rev. B **92**, 245410 (2015).
[28] A. D. Kovacs, G. David, B. Dora, and J. Cserti, Phys. Rev. B **95**, 035414 (2017).
[29] E. Illes and E. J. Nicol, Phys. Rev. B **94**, 125435 (2016).
[30] T. Biswas and T. K. Ghosh, J. Phys.: Condens. Matter **28**, 495302 (2016).
[31] Y. Xu and L.-M. Duan, Phys. Rev. B **96**, 155301 (2017).
[32] SK Firoz Islam and P. Dutta, Phys. Rev. B **96**, 045418 (2017).
[33] E. Illes and E. J. Nicol, Phys. Rev. B **95**, 235432 (2017).
[34] T. Biswas and T. K. Ghosh, J. Phys.: Condens. Matter **30**, 075301 (2018).
[35] D. Xiao, M. C. Chang, and Q. Niu, Rev. Mod. Phys. **82**, 1959 (2010).

[36] The eigenspectrum of the unscaled Hamiltonian is $\lambda_0 = 0$, $\lambda_\pm = \pm|f_{\mathbf{k}}|\sqrt{t_{AB}^2 + t_{BC}^2}$. For a fixed $\mathbf{k}$, $\lambda_\pm$ is determined by the points in two-dimensional Euclidean parameter space of hopping amplitudes t_{AB} and t_{BC}. Since $\lambda_\pm$ is proportional to $\sqrt{t_{AB}^2 + t_{BC}^2}$, the spectrum will be invariant for all points lying on a circle of fixed radius centered at origin. Rescaling the Hamiltonian by

$\cos\phi$ is equivalent to parametrizing the hopping amplitudes as $t_{AB} = t\cos\phi$ and $t_{BC} = t\sin\phi$ such that $\tan\phi = t_{BC}/t_{AB} = \alpha$. As a result, variation of α or ϕ traces out the points on a circle of radius t in the parameter space such that the eigenvalues are independent of α.

[37] E. Dagotto, E. Fradkin, and A. Moreo, Phys. Lett. B **172**, 383 (1986).

[38] R. Shen, L. B. Shao, B. Wang, and D. Y. Xing, Phys. Rev. B **81**, 041410(R) (2010).

[39] V. Apaja, M. Hyrkäs, and M. Manninen, Phys. Rev. A **82**, 041402(R) (2010).

[40] N. Goldman, D. F. Urban, and D. Bercioux, Phys. Rev. A **83**, 063601 (2011).

[41] D. Green, L. Santos, and C. Chamon, Phys. Rev. B **82**, 075104 (2010).

[42] R. A. Vicencio, C. Cantillano, L. Morales-Inostroza, B. Real, C. Mejia-Cortes, S. Weimann, A. Szameit, and M. I. Molina, Phys. Rev. Lett. **114**, 245503 (2015).

[43] S. Mukherjee, A. Spracklen, D. Choudhury, N. Goldman, P. Ohberg, E. Andersson, and R. R. Thomson, Phys. Rev. Lett. **114**, 245504 (2015).

[44] M. Holthaus and D. W. Hone, Phys. Rev. B **49**, 16605 (1994).

[45] M. Grifoni and P. Hanggi, Phys. Rep. **304**, 229 (1998).

[46] F. H. M. Faisal and J. Z. Kaminski, Phys. Rev. A **54**, R1769 (1996); **56**, 748 (1997).

[47] H. Hsu and L. E. Reichl, Phys. Rev. B **74**, 115406 (2006).

[48] D. F. Martinez, L. E. Reichl, and G. A. Luna-Acosta, Phys. Rev. B **66**, 174306 (2002).

[49] Y. H. Wang, H. Steinberg, P. Jarillo-Herrero, and N. Gedik, Science **342**, 453 (2013).